Chaos ARTICLE scitation.org/journal/cha

Partial synchronization in the second-order Kuramoto model: An auxiliary system method

Cite as: Chaos **31**, 113113 (2021); doi: 10.1063/5.0066663
Submitted: 11 August 2021 · Accepted: 11 October 2021 ·
Published Online: 9 November 2021

View Online Export Citation CrossMark

Nikita V. Barabash,[1,2,a] Vladimir N. Belykh,[1,2,b] Grigory V. Osipov,[2,c] and Igor V. Belykh[2,3,d]

AFFILIATIONS

[1] Department of Mathematics, Volga State University of Water Transport, 5A, Nesterov str., Nizhny Novgorod 603950, Russia
[2] Department of Control Theory, Lobachevsky State University of Nizhny Novgorod, 23, Gagarin Ave., 603950 Nizhny Novgorod, Russia
[3] Department of Mathematics and Statistics, Georgia State University, P.O. Box 4110, Atlanta, Georgia 30302-410, USA

Note: This paper is part of the Focus Issue, In Memory of Vadim S. Anishchenko: Statistical Physics and Nonlinear Dynamics of Complex Systems.
[a] **Electronic mail:** barabash@itmm.unn.ru
[b] **Electronic mail:** belykh@unn.ru
[c] **Electronic mail:** osipov@itmm.unn.ru
[d] **Author to whom correspondence should be addressed:** ibelykh@gsu.edu

ABSTRACT

Partial synchronization emerges in an oscillator network when the network splits into clusters of coherent and incoherent oscillators. Here, we analyze the stability of partial synchronization in the second-order finite-dimensional Kuramoto model of heterogeneous oscillators with inertia. Toward this goal, we develop an auxiliary system method that is based on the analysis of a two-dimensional piecewise-smooth system whose trajectories govern oscillating dynamics of phase differences between oscillators in the coherent cluster. Through a qualitative bifurcation analysis of the auxiliary system, we derive explicit bounds that relate the maximum natural frequency mismatch, inertia, and the network size that can support stable partial synchronization. In particular, we predict threshold-like stability loss of partial synchronization caused by increasing inertia. Our auxiliary system method is potentially applicable to cluster synchronization with multiple coherent clusters and more complex network topology.

Clusters of synchronized oscillators are observed in a variety of natural and man-made networks. Yet, it has been difficult to fully understand the conditions under which such clusters form. Partial synchronization, in which some heterogeneous oscillators synchronize in a group while the others remain incoherent, is an important example of such cluster synchronization that could allow an analytical treatment of its stability. In this paper, we perform such an analytical study for the Kuramoto model with inertia. We seek to understand a complex interplay between oscillator heterogeneity, inertia, and the sizes of coherent and incoherent clusters that controls the stability of partial synchronization. While the existing methods for assessing the stability of partial synchronization in Kuramoto networks typically rely on the assumption of an infinitely large network size, there is a lack of rigorous methods that can handle finite-size Kuramoto networks. Here, we close this gap by developing an auxiliary system method that effectively characterizes multi-dimensional intra-phase and inter-cluster dynamics by means of a two-dimensional pendulum-type auxiliary system. In particular, our method reveals a threshold-like connection between permissible natural frequency mismatch, inertia, and partial synchronization. Our results may also give an insight into the role of inertia in the creation of a stable chimera in networks of identical oscillators which is a direct, albeit surprising analog of partial synchronization among heterogeneous oscillators.

I. INTRODUCTION

Synchronization of oscillatory rhythms has been shown to be critical for the functioning of neuronal, biological, and engineering networks.[1–8] Complete synchronization and cluster synchronization are the most notable forms of synchronized oscillatory rhythms. The stability of complete synchronization of identical or nearly identical oscillators heavily depends on the underlying network topology.[9–13] Cluster synchronization is observed when the network splits into clusters of coherent oscillators but there is no synchronization between the clusters.[14–24] The existence of clusters of perfect synchrony in networks of identical oscillators is determined by intrinsic symmetries of the network.[22,25] The stability of such cluster synchronization[14,16,17,21,24] and its persistence against oscillators' parameter detuning[18] have received a great deal of attention in the literature.

The Kuramoto model of first-order phase oscillators with an all-to-all coupling[26,27] is the classical, analytically tractable example of a network that can exhibit different forms of transition from total incoherence to cluster and complete synchronization.[28–35] In the case of heterogeneous phase oscillators, the most common spatiotemporal pattern that emerges on the way to complete synchronization is partial synchronization in which some oscillators synchronize within a cluster, whereas the remaining asynchronous oscillators form an incoherent state.[28,36,37] The extension of partial synchronization to identical oscillators has led to the discovery of chimera states in which even structurally and dynamically identical oscillators can break into two coherent and incoherent states.[38–41] Originally discovered in the Kuramoto model, chimera states have been found in other networks of excitable systems,[41–46] including networks of mechanical oscillators,[47] coupled pendula,[48] pedestrians on a wobbly bridge,[49] optical systems,[50] coupled chemical oscillators,[51] and spatially extended continuous systems.[52] Proving the stability of chimera states even in the more analytically tractable classical Kuramoto model is a challenging problem. Therefore, most existing studies are purely numerical, with a few exceptions of a more rigorous analysis of chimera states in large networks[53–55] and "weak" chimeras in small networks.[56,57]

The second-order Kuramoto model of 2D oscillators with inertia[58] is often a better alternative to the classical first-order Kuramoto model for describing partial synchronization and chimera states in real-world networks of oscillators that can adjust their natural frequencies (power grid systems are a case in point[59]). Due to the presence of inertia that increases the dimensionality of the intrinsic oscillator dynamics, cooperative dynamics of the second-order Kuramoto model is much richer[60–64] and includes intermittent chaotic chimeras,[65] inertia-induced hysteretic transitions from incoherence to coherence,[66] bistability of synchronous clusters,[67] solitary states,[68,69] and chaotic inter-cluster dynamics.[70] Partial synchronization in the second-order Kuramoto model of heterogeneous oscillators has been previously studied through the lens of mean-field theory under the assumption of an infinitely large network size.[66] Similarly, the stability of the stronger form of partial synchronization, two-cluster synchronization in which heterogeneous oscillators synchronize within two distinct clusters has been analyzed in the second-order Kuramoto model on random graphs in the limit of infinitely large networks and a continuous bimodal distribution.[71] This limit allowed for an effective reduction of the stability problem to a set of a low-dimensional ordinary differential equation and two Vlasov partial differential equations.[71] Back to the study of partial synchronization in the classical heterogeneous first-order Kuramoto model, the assumption of the continuum limit has also enabled the use of the Ott–Antonsen ansatz to obtain exact results on chimera-like partial synchronization.[72]

In this paper, we seek to relax these limits toward developing a method for proving stability of partial synchronization in the finite-dimensional second-order Kuramoto model. Our method utilizes a 2D pendulum-type piecewise-smooth system to separate the dynamics of the coherent and incoherent clusters and bound the oscillating phase differences between oscillators within the coherent cluster. This method is a non-trivial extension of the qualitative techniques, previously developed for Kuramoto networks,[70,73] in the direction of partial synchronization of heterogeneous Kuramoto oscillators with inertia. We perform a detailed qualitative bifurcation analysis of the auxiliary system and derive explicit bounds on the maximum natural frequency mismatch, inertia, and the relative size of the coherent and incoherent clusters that support stable partial synchronization. In particular, our analytical study indicates the existence of an effective lower bound for moderately large inertia beyond which inertia does not essentially affect the stability of partial synchronization.

The layout of this paper is as follows. In Sec. II, we introduce the oscillator network model and give our definition of partial synchronization. In Sec. III, we derive the auxiliary system and perform its qualitative bifurcation analysis, which yields sufficient conditions on the existence and size of a trapping region that restricts the dynamics of oscillators' phase differences. In Sec. IV, we return to partial synchronization in the original system to formulate the main result of the paper. In Sec. V, we provide concluding remarks and discuss potential applicability of the proposed method to other types of cluster synchronization and network topology.

II. THE SECOND-ORDER KURAMOTO MODEL

We consider the second-order Kuramoto model of N phase oscillators with inertia,

$$\beta\ddot{\varphi}_i + \dot{\varphi}_i = \omega_i + \frac{K}{N}\sum_{j=1}^{N}\sin(\varphi_j - \varphi_i), \quad i = 1, 2, \ldots, N, \tag{1}$$

where $\varphi_i \in [0, 2\pi]$ is the phase of the ith oscillator, parameter $\beta > 0$ represents inertia, and parameter $K > 0$ is a coupling strength corresponding to an all-to-all network topology. The oscillators have heterogeneous intrinsic frequencies ω_i, $i = 1, .., N$ that are chosen from a discrete bimodal distribution. We also allow time-dependent frequencies $\omega_i(t)$ that may vary within constraints to be imposed.

We seek to identify the maximum range of frequencies ω_i and its dependence on inertia β that yield stable partial synchronization in which first N_{osc} oscillators with ω_i, $i = 1, \ldots, N_{osc}$ synchronize to a common frequency and form coherent cluster C_{osc}, whereas the remaining N_{rot} oscillators maintain heterogeneous frequencies and form incoherent cluster C_{rot}.

More precisely, stable synchronization between any pair of oscillators i and j within coherent cluster C_{osc} is said to occur when

$$|\varphi_i(t) - \varphi_j(t)| < \varepsilon \quad \text{for} \quad \forall t > 0, \tag{2}$$

where parameter $\varepsilon \in (0, \pi]$ is the maximum allowed phase difference. Note that this type of synchronization allows the phase differences to oscillate in time within the bounds constrained by

ε. In the most general case of $\varepsilon = \pi$, which yields the maximum phase difference of π that still prevents phase difference slips and rotations, the synchronization is defined in its broadest sense. In the following, we will reveal the role of ε in the stability of coherent cluster C_{osc}. For this purpose, we shall introduce the notion of *ε-synchronization* as determined in (2) for chosen $\varepsilon < \pi$. It follows from (2) that the frequencies of oscillators within coherent cluster C_{osc} become equal so that $\langle\dot{\varphi}_i\rangle = \langle\dot{\varphi}_j\rangle$, where $\langle\cdots\rangle$ denotes a time average. Similarly, a whirling phase difference between any pair of oscillator k from incoherent cluster C_{rot} and oscillator i from coherent cluster C_{osc} induces desynchronization between the clusters so that $\langle\dot{\varphi}_i - \dot{\varphi}_k\rangle \neq 0$. This definition of partial ε-synchronization will be made more precise in Sec. III. Note that this definition does not specify phase relations between oscillators within incoherent cluster C_{rot} whose rotating phases may become synchronized. As a result, we tend to apply the term "incoherent" cluster to C_{rot} somewhat loosely, although all numerical simulations performed to validate our analytical bounds and presented in Sec. IV suggest that cluster C_{rot} is indeed incoherent for the chosen wide range of parameters and initial conditions.

III. AUXILIARY SYSTEM METHOD

In this section, we develop the auxiliary system method for deriving sufficient conditions for frequency mismatches and inertia that maintain stable partial synchronization.

A. Transformation to coupled pendulum-type equations

Introducing new variables for phase differences between any pair of oscillators,

$$\theta_{ij} = \frac{\varphi_i - \varphi_j}{2}, \quad i,j = 1,\ldots,N \tag{3}$$

and rescaling the parameters and time, we transform system (1) into the form

$$\ddot{\theta}_{ij} + \lambda\dot{\theta}_{ij} = \Delta_{ij} + \frac{1}{2N}\sum_{k=1}^{N}(\sin 2\theta_{ki} - \sin 2\theta_{kj}), \quad i,j = 1,\ldots,N, \tag{4}$$

where the derivatives are calculated with respect to new time $\tau = \sqrt{K/\beta}\,t$, $\Delta_{ij} = \dfrac{\omega_i - \omega_j}{2K}$ represents normalized frequency differences, and $\lambda = \dfrac{1}{\sqrt{\beta K}}$ is a damping parameter. Using the sum-to-product trigonometric identity $\sin 2\theta_{ki} - \sin 2\theta_{kj} = 2\cos(\theta_{ki} + \theta_{kj})\sin(\theta_{ki} - \theta_{kj})$ and noting that $\theta_{ki} - \theta_{kj} = -\theta_{ij}$, we rewrite system (4) in a more convenient form

$$\ddot{\theta}_{ij} + \lambda\dot{\theta}_{ij} = \Delta_{ij} - F_{ij}\sin\theta_{ij}, \quad i,j = 1,2,\ldots,N, \tag{5}$$

where

$$F_{ij} = \frac{1}{N}\sum_{k=1}^{N}\cos(\theta_{ki} + \theta_{kj}), \quad i,j = 1,\ldots,N \tag{6}$$

is a function of time-varying phase differences.

System (5) may be viewed as a system of coupled pendulum equations whose dynamics can be qualitatively studied in terms of limit sets of the damped pendulum equation with constant torque.[74] Toward this goal, we rewrite (5) as

$$\begin{aligned} \dot{\theta}_{ij} &= y_{ij}, \\ \dot{y}_{ij} &= -\lambda y_{ij} + \Delta_{ij} - F_{ij}\sin\theta_{ij}, \quad i,j = 1,2,\ldots,N. \end{aligned} \tag{7}$$

To analyze ε-synchronization between oscillators i and j within coherent cluster C_{osc}, we consider a subset of Eq. (7) that corresponds to phase differences θ_{ij}, $i,j = 1,..,N_{osc}$ that belong to C_{osc}. For this subset of equations, we split functions F_{ij} into two parts, corresponding to the connections within coherent cluster C_{osc} and with oscillators from incoherent cluster C_{rot},

$$F_{ij} = \frac{1}{N}\sum_{k=1}^{N_{osc}}\cos(\theta_{ki} + \theta_{kj}) + \frac{1}{N}\sum_{k=N_{osc}+1}^{N}\cos(\theta_{ki} + \theta_{kj}), \quad i,j = 1,\ldots,N_{osc}, \tag{8}$$

where we have rearranged the oscillator indexes so that first $k = 1,..,N_{osc}$ oscillators belong to coherent cluster C_{osc}, whereas the remaining $k = N_{osc}+1,..,N$ oscillators determine incoherent cluster C_{rot}.

Definition 1. *Partial ε-synchronization in system (7) is stable if for any time $t > 0$,*

$$\begin{aligned} &|\theta_{ij}(t)| < \varepsilon/2, \quad for \quad i,j = 1,\ldots,N_{osc}, \\ &\dot{\theta}_{ik}(t) > 0, \quad i = 1,\ldots,N_{osc}, \quad k = N_{osc}+1,\ldots,N. \end{aligned} \tag{9}$$

This definition of partial ε-synchronization is convenient for rigorous stability studies. However, it might appear too restrictive in the broader context of partial synchronization in which whirling oscillators within the incoherent cluster may exhibit occasional phase slips, thereby violating the second condition in (9).

According to Definition 1, stable partial ε-synchronization places bounds on the sums in (8) so that ε-synchronized oscillators within coherent cluster C_{osc} yield $\cos(\theta_{ki} + \theta_{kj}) > \cos\varepsilon$ in the first sum, while the cosine term in the second sum corresponding to connections of C_{osc} to oscillators from C_{rot} is simply bounded via $|\cos(\theta_{ki} + \theta_{kj})| < \cos 2\pi = 1$. Thus, the time evolution of functions F_{ij} is restricted by

$$\begin{aligned} a < F_{ij} \le 1 \quad &\text{for} \quad i,j = 1,\ldots,N_{osc}, \\ |F_{ik}| \le 1 \quad &\text{for} \quad i = 1,\ldots,N_{osc}, \\ & \qquad\quad k = N_{osc}+1,\ldots,N, \end{aligned} \tag{10}$$

where parameter a is defined as

$$a = \frac{1}{N}\left(N_{osc}\cos\varepsilon - N_{rot}\right). \tag{11}$$

Therefore, by virtue of (10), the right-hand sides of $\dot{y}_{ij}$ in (7) for $i,j = 1,\ldots,N_{osc}$ are bounded so that

$$A_{ij}^{-} < \dot{y}_{ij} \le A_{ij}^{+}, \tag{12}$$

where

$$A_{ij}^{-}=\begin{cases}\Delta_{ij}-\lambda y_{ij}-a\sin\theta_{ij} & \text{for} \quad -\pi\le\theta_{ij}<0,\\ \Delta_{ij}-\lambda y_{ij}-\sin\theta_{ij} & \text{for} \quad 0\le\theta_{ij}<\pi,\end{cases}$$
$$A_{ij}^{+}=\begin{cases}\Delta_{ij}-\lambda y_{ij}-\sin\theta_{ij} & \text{for} \quad -\pi\le\theta_{ij}<0,\\ \Delta_{ij}-\lambda y_{ij}-a\sin\theta_{ij} & \text{for} \quad 0\le\theta_{ij}<\pi.\end{cases} \tag{13}$$

To place uniform bounds on the dynamics of each system $(\dot{\theta}_{ij},\dot{y}_{ij})$ from (7) with $i,j=1,\ldots,N_{osc}$, we introduce the auxiliary system

$$\begin{aligned}&\dot{\theta}=y \\ &\dot{y}=A^{+}\end{aligned}\quad \text{for} \quad y\ge 0,$$
$$\begin{aligned}&\dot{\theta}=y \\ &\dot{y}=A^{-}\end{aligned}\quad \text{for} \quad y\le 0, \tag{14}$$

where

$$A^{+}=\begin{cases}\Delta-\lambda y-\sin\theta & \text{for} \quad -\pi\le\theta<0,\\ \Delta-\lambda y-a\sin\theta & \text{for} \quad 0\le\theta<\pi,\end{cases}$$
$$A^{-}=\begin{cases}-\Delta-\lambda y-a\sin\theta & \text{for} \quad -\pi\le\theta<0,\\ -\Delta-\lambda y-\sin\theta & \text{for} \quad 0\le\theta<\pi,\end{cases} \tag{15}$$

and

$$\Delta=\max_{ij}|\Delta_{ij}| \quad \text{for} \quad i,j=1,\ldots,N_{osc} \tag{16}$$

is the maximum normalized frequency mismatch between two oscillators within coherent cluster C_{osc}. Note that auxiliary system (14) is obtained from (13) by removing the subscripts and replacing $\Delta_{ij}\in[-\Delta,\Delta]$ with bounds $-\Delta$ and Δ.

In the following, we will derive conditions under which trajectories of auxiliary system (14) form trapping region G_{trap} for the trajectories of systems $(\dot{\theta}_{ij},\dot{y}_{ij})$ from (7) with $i,j=1,\ldots,N_{osc}$. The size of trapping region G_{trap} will determine maximum frequency mismatch Δ that allows ε-synchronization within coherent cluster C_{osc}.

Note that using bounds (13)–(15), we decouple systems $(\dot{\theta}_{ij},\dot{y}_{ij})$ with $i,j=1,\ldots,N_{osc}$, thereby reducing the analysis of full coupled system (7) to a set of independent 2D pendulum-type equations. By doing so, we will also separate the conditions for stable ε-synchronization within C_{osc} from the conditions for the oscillators from incoherent cluster C_{rot} to maintain whirling phase differences with cluster C_{osc}. The latter condition can be easily fulfilled by choosing the minimum normalized frequency mismatch between oscillators i from coherent cluster C_{osc} and k from incoherent cluster C_{rot}

$$\delta=\min_{ik}\Delta_{ik}>1 \quad \text{for} \quad \begin{aligned}&i=1,\ldots,N_{osc},\\ &k=N_{osc}+1,\ldots,N.\end{aligned} \tag{17}$$

Indeed, as $|F_{ik}|\le 1$, for $i=1,\ldots,N_{osc}$, $k=N_{osc}+1,\ldots,N$, the right-hand sides of ik subsystems in (5) are always positive for $\delta>1$, thereby yielding only whirling phase differences.

Therefore, to derive sufficient conditions for partial ε-synchronization, it remains to characterize possible dynamics of auxiliary system (14) and determine bounds on Δ,λ, and ε that guarantee ε-synchronization within C_{osc}.

B. Dynamics of the piecewise-smooth auxiliary system

Auxiliary system (14) is a 2D piecewise-smooth system, which is composed from four pendulum equations determining distinct dynamics in each quadrant of the (θ,y)-plane. System (14) is invariant under the involution $(\theta,y,\Delta)\to(-\theta,-y,-\Delta)$. In terms of the (θ,y) phase portrait, this odd symmetry implies that the system's trajectories for $y<0$ are simply the images of the trajectories for $y>0$, obtained by reflecting the trajectories about the θ and y coordinate axes.

When they exist, fixed points of (14) lie on discontinuity line $y=0$. Each of the four pendulum systems may have up to two fixed points, yielding a total of four fixed points due to the symmetry. More specifically, pendulum system A^{+} has two fixed points

$$e_1\left(\theta_{e_1}=\arcsin\frac{\Delta}{a},0\right),\quad s_1\left(\theta_{s_1}=\pi-\arcsin\frac{\Delta}{a},0\right) \tag{18}$$

that lie in the region $0\le\theta<\pi$. Due to the odd symmetry, system A^{-} also has two fixed points

$$e_2\left(\theta_{e_2}=-\arcsin\frac{\Delta}{a},0\right),\quad s_2\left(\theta_{s_2}=-\pi+\arcsin\frac{\Delta}{a},0\right) \tag{19}$$

that belong to the region $-\pi\le\theta<0$. In systems A^{+} and A^{-}, $e_{1,2}$ are stable fixed points and $s_{1,2}$ are saddles. It is important to emphasize that when combined together in piecewise-smooth auxiliary system (14), these four fixed points change their types and stability according to the following properties.

Property 1. For $y=+0$, the vector field of auxiliary system (14) is determined by system A^{+} with $y=0$ and, therefore, $\dot{y}|_{y=+0}<0$ along line segment S_{e_1,s_1} connecting points e_1 and s_1 and $\dot{y}|_{y=+0}>0$ along the line segment connecting points e_1 and $s_1-2\pi$.

Property 2. For $y=-0$, the vector field of auxiliary system (14) is determined by system A^{-} with $y=0$ and, therefore, $\dot{y}|_{y=-0}<0$ along line segment S_{e_2,s_2} connecting points e_2 and s_2 and $\dot{y}|_{y=-0}<0$ along the line segment connecting points e_2 and $s_2+2\pi$.

Property 3. Combining the mutual arrangements of the vector fields from Properties 1 and 2, one concludes that points e_1 and e_2 become half-stable, attracting (repelling) trajectories from the $y>0$ $(y<0)$ region. Line segment S_{e_1,e_2} between fixed points e_1 and e_2 represent unstable sliding motions. Similarly, points s_1 and s_2 become pseudo-saddles with the part of discontinuity line $y=0$ between points s_1 and $s_2+2\pi$ corresponding to unstable sliding motions and playing the role of a separatrix [Fig. 2(b)].

The reader should not be surprised by these unusual transformations that originate from the piecewise-smooth nature of auxiliary system (14) as piecewise-smooth systems often exhibit dynamics and bifurcations impossible in their smooth counterparts.[75–77] It should be noted that there is no strict one-to-one relation between the dynamics of the non-smooth auxiliary system (14) and original smooth system (1). However, piecewise-smooth heteroclinic contours and limit cycles of auxiliary system (14) serve as constructive bounds for smooth trajectories of the original system (1).

Our approach to deriving bounds on the dynamics of the original system (7) is based on the property that the vector flow of auxiliary system (14) is transversal to any non-trivial trajectory of

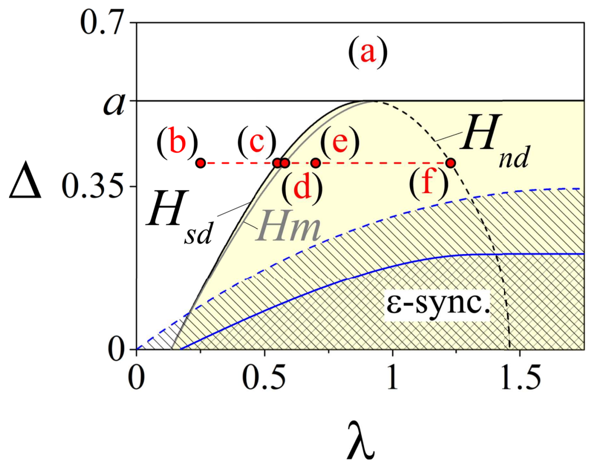

FIG. 1. Numerically validated bifurcation diagram of auxiliary system (14) (an illustration of Propositions 1–4). The yellow region bounded by curve H_{sd} and line $\Delta = a$ corresponds to the existence of trapping region G_{trap}. Curve H_{sd} corresponds to a heteroclinic bifurcation that forms heteroclinic contour L^{∞}_{sd}. Line $\Delta = a$ indicates a saddle-node bifurcation at which fixed points e_1 and s_1 (e_2 and s_2) merge together and disappear. Curve Hm corresponds to a homoclinic bifurcation of saddle s_1 (and of s_2). Curve H_{nd} displays a heteroclinic bifurcation that yields heteroclinic contour L^{∞}_{nd}. The red dashed line with points (b)–(f) exemplifies the evolution of phase dynamics as a function of λ for a fixed Δ. Points (a)–(f) correspond to subplots (a)–(f) of Fig. 2. The blue solid curve is a combined graph of functions (21) and (22) with fixed $d_G = \varepsilon = \pi/4$, bounding the parameter region (double dashed) where the numerically validated conditions of Proposition 3 for auxiliary system (14) support partial ε-synchronization. The blue dashed curve, calculated for original system (1), bounds the actual parameter region (dashed) for partial ε-synchronization in system (1). Other parameters are $N_{osc} = 90$, $N_{rot} = 10$ yielding $a = 0.536$ for $\varepsilon = \pi/4$.

each $(\dot{\theta}_{ij}, \dot{y}_{ij})$ system from (7). More precisely, the vertical component of vector fields $(\dot{\theta}, \dot{y})$ of systems A^+ and A^- is larger than that of vector fields $(\dot{\theta}_{ij}, \dot{y}_{ij})$ in (7), except for the fixed points. Therefore, the trajectories of the $(\dot{\theta}_{ij}, \dot{y}_{ij})$ systems cross the trajectories of system A^+ and A^- in the downward and upward directions, respectively. As a result, oscillatory limit cycles and heteroclinic contours in auxiliary system (7) can form a trapping region for trajectories of each $(\dot{\theta}_{ij}, \dot{y}_{ij})$ system, thereby restricting their dynamics. In the following, we will qualitatively and quantitatively characterize the (λ, Δ)-bifurcation diagram of Fig. 1 that indicates the parameter regions in which the trapping region exists.

Toward this goal, we apply the results from Belyustina and Belykh[78] on a qualitative bifurcation analysis of a pendulum-type system on a cylinder that can be written in terms of auxiliary system (14) as follows:

$$\dot{\theta} = y,$$
$$\dot{y} = \gamma - \lambda y - aF(\theta), \tag{20}$$

where $\gamma > 0$ is a new parameter representing constant torque and periodic function $F(\theta) = F(\theta + 2\pi)$ with zero mean may be piecewise-smooth and must satisfy the following properties: $F(\theta) \in C^1$ for $\theta \in [0, 2\pi)$, where $\theta \neq \theta^{(h)}$ $(h = 1, \ldots, n)$, $F(\theta^{(h)}) \in Lip$, $F_\theta(\theta) > 0$ for $\theta \in (-\theta_0, \theta_0)$, $F_\theta(\theta) < 0$ for $\theta \in (\theta_0, 2\pi - \theta_0)$, $F(\theta_0) = 1$, and $\max |F_\theta(\theta)| = m$. The derivative $F_\theta(\theta)$ of piecewise-smooth function of $F(\theta)$ at n singularity points θ_h may be defined by any value lying between the left and right limits of $F_\theta(\theta)$. The simplest example of $F(\theta)$ that satisfies these conditions is $F(\theta) = \sin(\theta)$ that turns (20) into the standard damped pendulum equation with constant torque for $a = 1$. An important property of piecewise-function $F(\theta)$ is that its average value $\langle F(\theta)\rangle = \frac{1}{2\pi}\int_{-\pi}^{\pi} F(\theta)d\theta = 0$.

Theorem 5 from Belyustina and Belykh[78] guarantees that the (λ, γ)-parameter bifurcation diagram for piecewise-smooth system (20) is qualitatively similar to that of the classical pendulum equation with damping λ and constant torque γ. In particular, these results prove (i) the existence of a curve $\gamma = \gamma_{HM}(\lambda)$ that corresponds to a homoclinic bifurcation of the saddle fixed point of (20), and (ii) a saddle-node bifurcation at $\gamma = a + \dfrac{1-a}{2\pi}$. In terms of the (λ, γ)-parameter plane, the concave down graph of $\gamma = \gamma_{HM}(\lambda)$ emanates from the origin and joins horizontal line $\gamma = a + \dfrac{1-a}{2\pi}$ at some point, similar to homoclinic bifurcation curve $\gamma = T(\lambda)$, well approximated by[67] $T(\lambda) = \dfrac{4}{\pi}\lambda - 0.305\lambda^3$, which approaches saddle-node bifurcation line $\gamma = 1$ in the classical damped pendulum equation with constant torque.[74]

Going back to auxiliary system (14), we note that it belongs to the general system (20), provided that $\gamma = \Delta + \dfrac{1-r}{2\pi}$. This property is due to the fact that the average value of A^+ (and of A^-),

$$\langle A^+(\theta)\rangle = \frac{1}{2\pi}\int_{-\pi}^{\pi} A^+(\theta)\, d\theta$$
$$= \frac{1}{2\pi}\left[\int_{-\pi}^{0} \sin\theta\, d\theta + \int_{0}^{\pi} a\sin\theta\, d\theta\right] = -\frac{1-a}{2\pi}$$

is shifted from $\langle F(\theta)\rangle$ by a constant $(a-1)/(2\pi)$. Thus, auxiliary system (14) inherits the main bifurcation properties of system (20) such that its homoclinic bifurcation curve $\Delta = \Delta_{Hm}(\lambda)$ and saddle-node bifurcation $\Delta = a$ are identical to the corresponding curves of system (20), except for a vertical shift of $-\dfrac{1-a}{2\pi}$ (see curve Hm in Fig. 1). While we cannot determine the exact form of homoclinic bifurcation curve $\Delta = \Delta_H(\lambda)$ and identify the corresponding bifurcation value λ_{Hm} for a given Δ, we will use the existence of this curve as a qualitative reference for characterizing the locations of other bifurcation curves of system (14).

C. The existence and size of a trapping region

The following assertion gives the existence condition for trapping region G_{trap} and supports the bifurcation parameter partition for the dynamics of auxiliary system (14) given in Fig. 1. We define a trapping region as a compact subset of the auxiliary's system phase space such that every trajectory that starts within the trapping region remains there as the system evolves.

Proposition 1 (the existence of the trapping region). *A. For a fixed $\Delta < a$, trapping region G_{trap} (the yellow region in Fig. 2)*

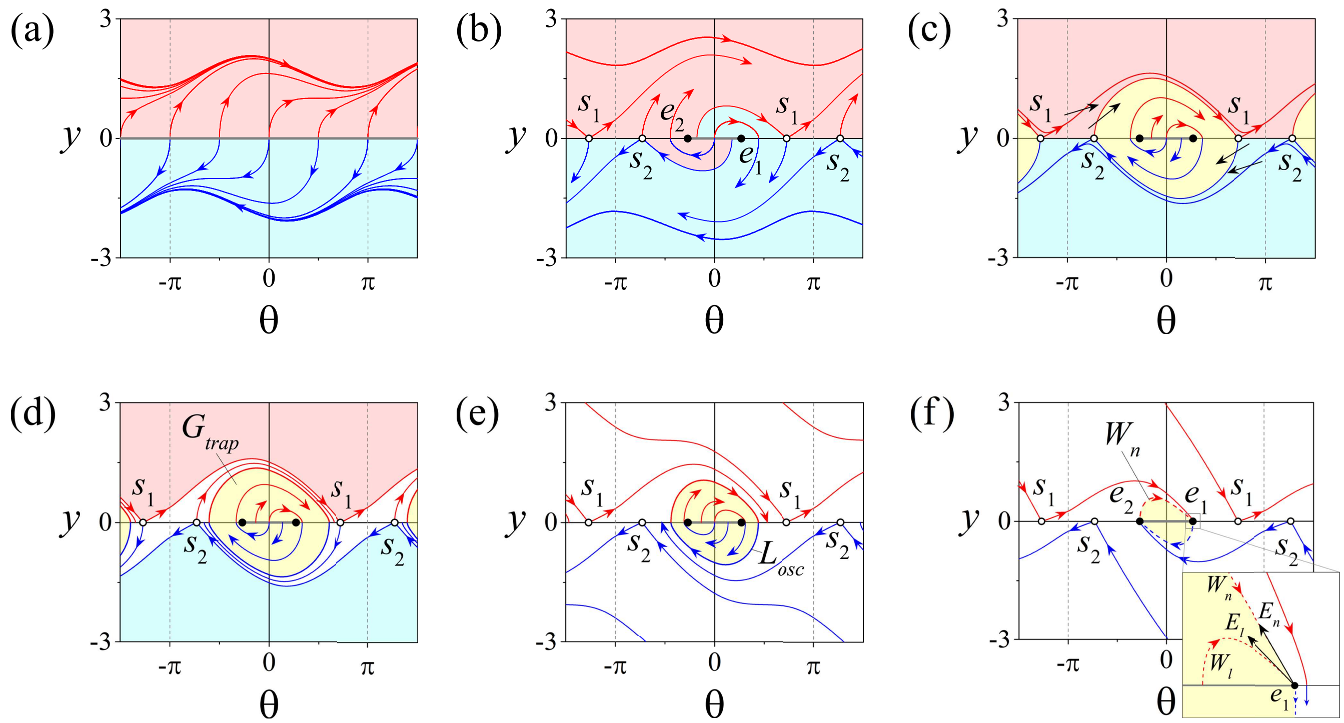

FIG. 2. The existence of trapping region G_{trap} (yellow region) and the evolution of its size in auxiliary system (14) (an illustration of Propositions 1 and 2). All trajectories are calculated numerically. Phase portrait (a) corresponds to parameter region (a) in Fig. 1 and displays two globally stable rotatory limit cycles (red and blue thick lines) with their attraction basins (light red and blue areas, respectively), yielding no trapping regions ($\lambda = 1$, $\Delta = 1.53$). Phase portraits (b)–(f) correspond to points (b)–(f) in Fig. 1 and are calculated as a function of λ for fixed $\Delta = 0.4$. Phase portrait (b) contains no trapping region and is similar to (a), expect for the presence of half-stable fixed points e_1, e_2, s_1, and s_2 ($\lambda = 0.25$). Phase portrait (c) corresponds to the formation of trapping region G_{trap} (yellow) via a heteroclinic bifurcation at which the stable manifolds of fixed points s_1 and s_2 form heteroclinic contour L^{∞}_{sd} (not marked) ($\lambda = \lambda_{Hsd} = 0.25$). This half-stable heteroclinic contour co-exists with the rotatory limit cycles preserved from (b). The black arrow lines indicate the direction of the vector field of corresponding pendulum system (7). Phase portrait (d) displays a homoclinic bifurcation that forms homoclinic orbit Hm (not marked) to each of fixed points s_1 and s_2 ($\lambda = \lambda_{Hm} = 0.580\,077$). This homoclinic orbit co-exists with a stable limit cycle bounding the trapping region (yellow) and born as a result of the heteroclinic bifurcation in (c). Phase portrait (e) corresponds to a non-bifurcation value of $\lambda = 0.7$ that preserves the stable limit cycle L_{osc} from (d) but makes it shrink in the size. Notice that the homoclinic bifurcation in (d) has led to the disappearance of the rotatory limit cycles. Phase portrait (f) corresponds to the formation of stable heteroclinic contour L^{∞}_{nd} (not marked) formed by stable non-leading manifold W_n (red dashed line) of fixed point e_1 starting from e_2 and its odd symmetric counterpart (blue dashed line) ($\lambda = \lambda_{Hnd} = 1.2271$). The inset shows a zoomed-in region around e_1 and displays the mutual arrangement of the stable non-leading (W_n) and leading (W_l) manifolds of e_1 and the unstable manifold of s_1 (red solid line). Black arrow lines E_l and E_n are the eigenvectors associated with eigenvalues $\kappa^{\pm}$ (24) of fixed point e_1. The heteroclinic contour of (f) with constant size d_G defined in (21) preserves for any $\lambda > \lambda_{Hnd}$ (not shown).

exists for any $\lambda \geq \lambda_{Hsd}$, where $\lambda_{Hsd} < \lambda_{Hm}$ is a bifurcation value corresponding to the formation of heteroclinic contour L^{∞}_{sd} from the stable manifolds of saddle points s_1 and s_2.

B. Trapping region G_{trap} does not exist for $\Delta > a$.

Proof. To prove Claim A, we depart from the phase portrait and mutual arrangement of trajectories at the homoclinic bifurcation at λ_{Hm}, which are guaranteed by Theorem 5 from Belyustina and Belykh.[78] This phase portrait is determined by the existence of a homoclinic orbit of saddle s_1 and its symmetric counterpart, a homoclinic orbit of saddle s_2. Half-stable fixed points e_1 and e_2 are encircled by stable oscillatory limit cycle L_{osc} [Fig. 2(d)]. This limit cycle is formed by two glued trajectories leaving the unstable segment of discontinuity line $y = 0$ between e_2 and s_2 for $y > 0$ and between e_1 and s_1 for $y < 0$, respectively (see Properties 1 and 2). Note that this limit cycle forms the desired trapping region G_{trap}. Due to the existence of the homoclinic orbit of saddle s_1 (s_2), the trajectory of system A^+ (A^-) that emanates from point s_2 for $y > 0$ (s_1 for $y < 0$) cannot reach saddle s_1 (s_2) and returns to discontinuity line $y = 0$ at a point $\theta < s_1$ ($\theta > s_2$).

Central to the proof of Claim A is the property that the vector field of auxiliary system (14) turns clockwise with increasing λ since $\partial(A^{\pm}/y)/\partial\lambda = -1 < 0$. Therefore, the vector field originally tangent to limit cycle L_{osc} turns clockwise and points inside L_{osc} with increasing λ, thereby shrinking the limit cycle. The monotonic clockwise turn of the vector field also provides a strict order in which the mutual arrangements of the stable and unstable manifolds of fixed points s_1 and s_2 and the stable manifolds of fixed points e_1 and e_2 can evolve. Using the phase portrait at $\lambda = \lambda_{Hm}$ as a reference, we first decrease λ to identify a bifurcation value of λ at which the limit cycle disappears. Note that decreasing λ turns the vector field counterclockwise, thereby (i) destroying the homoclinic orbit, (ii) giving birth to a stable rotatory limit cycle L_{rot} with $\theta(t) \in [-\pi, \pi]$, and making the oscillatory limit cycle gradually grow in size until it merges into heteroclinic contour L_{sd}^{∞}, representing an infinite-period limit cycle which is "glued" from two stable manifolds of saddles s_1 and s_2 at $\lambda = \lambda_{Hsd}$ [Fig. 2(c)]. This time, the trajectory of system A^+ that emanates from point $(s_2, 0)$ reaches saddle s_1 and becomes its stable manifold that in turn forms the upper part of heteroclinic contour L_{sd}^{∞} for $y > 0$. Similarly, the trajectory of system A^- that departs from point $(s_1, 0)$ becomes the stable manifold of saddle s_2 and completes the heteroclinic contour for $y < 0$. Note that further decrease of $\lambda < \lambda_{Hsd}$ induces an additional turn of the vector field that leads to the disappearance of heteroclinic contour L_{sd}^{∞}, and, therefore, of trapping region G_{trap} [Fig. 2(b)].

To complete the proof of Claim A, we need to show that increasing $\lambda > \lambda_{Hm}$ preserves trapping region G_{trap}, although the size of G_{trap} may vary. Again, we start from $\lambda = \lambda_{Hm}$ and begin increasing λ. This increase destroys the homoclinic orbit so that the unstable manifold of s_1 (s_2) lies below (above) the stable manifold of s_1 (s_2) in the region $[-\pi, \pi]$ and, therefore, hits discontinuity line $y = 0$ at a point p^+ (p^-) between fixed points e_1 and s_1 (e_2 and s_2) [see Fig. 2(e)]. Points p^+ and p^- [not labeled in Fig. 2(e)] bound the size of limit cycle L_{osc}. Indeed, the existence of a stable limit cycle is guaranteed since all trajectories of system A^+ initiating from the line segment of $y = 0$ between points p^+ and e_2 must return to the line segment of $y = 0$ between points p^- and e_1 for $y > 0$ due to Property 3. Therefore, there must exist a trajectory of system A^+ that matches its symmetrical counterpart in system A^- to close the loop and form stable limit cycle L_{osc} that yields trapping region G_{trap}. Note that half-stable fixed points e_1 and e_2 of auxiliary system (14) encircled by stable limit cycle L_{osc} may be both stable foci or stable nodes of the corresponding systems A^+ and A^-. Indeed, these fixed points are stable foci at $\lambda = \lambda_{Hm}$ and turn into stable nodes at $\lambda = \lambda_{dn} > \lambda_{Hm}$ corresponding to the formation of a degenerate node (hence, the notation). The explicit value of λ_{dn} will be given in (23). Critical to our further bifurcation transition is the mutual arrangement between the trajectory T_{e_2} emanating from point e_2 for $y > 0$ and the stronger (non-leading) stable manifold W_n of stable node e_1 of system A^+. It is important to emphasize that as long as stable limit cycle L_{osc} exists, the trajectory T_{e_2} terminates at it and lies above the stable manifold W_n of e_1. The weaker (leading) stable manifold W_l always lies below the non-leading manifold W_n in the (θ, y) plane. This arrangement will be detailed through the calculation of the corresponding eigenvectors in the proof of Proposition 3 and is shown in Fig. 2(f).

Increasing λ decreases the gap between the critical trajectory T_{e_2} and the non-leading stable manifold W_n, while preserving stable limit cycle L_{osc} up to bifurcation value $\lambda = \lambda_{Hnd}$. At this value, the gap disappears so that trajectory T_{e_2} and manifold W_n merge together [Fig. 2(f)]. Similarly, their odd symmetrical counterparts of system A^-, the trajectory T_{e_1} emanating from point $(e_1, 0)$ for $y < 0$ and the non-leading stable manifold of fixed point e_2 join each other. This leads to the formation of a stable heteroclinic contour between half-stable fixed points e_1 and e_2 of auxiliary system (14) and the disappearance of stable limit cycle L_{osc}. Note that fixed points e_1 and e_2 are stable *nodes* of systems A^+ and A^-, respectively, so that we have termed this heteroclinic contour as heteroclinic "node" contour L_{nd}^{∞} to distinguish it from heteroclinic contour L_{sd}^{∞}, formed from two *saddles* s_1 and s_2 and depicted in Fig. 2(c).

Note that heteroclinic contour L_{nd}^{∞} representing trapping zone G_{trap} is preserved for any value $\lambda > \lambda_{Hnd}$. Indeed, increasing λ beyond λ_{Hnd} splits the trajectory T_{e_1} and the non-leading manifold W_n so that trajectory T_{e_1} is located under W_n. Confined between W_n and unstable sliding motion segment S_{e_1,e_2}, the trajectory T_{e_1} always approaches fixed point e_1, thereby forming the upper part of heteroclinic contour L_{nd}^{∞} for $y > 0$. Similarly, its odd symmetric image T_{e_2} forms the lower part of L_{nd}^{∞} for $y < 0$. This completes the proof of Claim A.

The proof of Claim B is straightforward. Fixed points e_1, s_1, e_2, s_2 do not exist for $\Delta > a$ and, therefore, oscillatory limit cycles or heteroclinic contours that yield trapping regions cannot exist. The dynamics of auxiliary system (14) is governed by two globally stable rotatory limit cycles [Fig. 2(a)]. □

Proposition 2 (the size of trapping region G_{trap}). *A. For $\Delta < a$ and $\lambda \geq \lambda_{Hnd}$, where λ_{Hnd} is a bifurcation value corresponding to the formation of heteroclinic contour L_{nd}^{∞}, detailed in the proof of Proposition 1, the size of trapping region G_{trap} in the θ direction is determined by the coordinates of fixed points e_1 and e_2 and equals*

$$d_G = 2 \arcsin \frac{\Delta}{a}. \tag{21}$$

B. For $\Delta < a$ and $\lambda_{Hsd} \leq \lambda < \lambda_{Hnd}$, the size of trapping region G_{trap} is defined by

$$d_G = f(\lambda, \Delta), \tag{22}$$

where function $f(\lambda, \Delta)$ monotonically decreases with increasing $\lambda \in [\lambda_{Hsd}, \lambda_{Hnd})$ and monotonically increases with increasing $\Delta \in [0, a)$, and $f(\lambda, 0) = 0$.

Proof. It follows from the proof of Proposition 1 that for $\Delta < a$ and $\lambda \geq \lambda_{Hnd}$ trapping domain G_{trap} is represented by heteroclinic contour L_{nd}^{∞} whose size d_G in the θ is the distance between fixed points e_1 and e_2. Therefore, by virtue of (18) and (19), $d_G = 2 \arcsin \frac{\Delta}{a}$. This completes the proof of Claim A.

The proof of Claim B is based on the properties revealed in the proof of Proposition 1 that the destruction of heteroclinic contour L_{nd}^{∞} by decreasing $\lambda < \lambda_{Hnd}$ at a fixed $\Delta^* < a$ gives birth to oscillatory limit cycle L_{osc} whose θ amplitude is larger than θ_{e_1}. Moreover, due to the monotonically increasing counterclockwise turn of the vector field with further decreasing λ, the amplitude of limit cycle L_{osc} monotonically increases until decreasing λ reaches its bifurcation value λ_{Hsd} at which the limit cycle ceases to exist. This indicates that the size of trapping region d_G, determined by the double θ amplitude of limit cycle L_{osc}, is a monotonically decreasing function in the interval $\lambda \in [\lambda_{Hsd}, \lambda_{Hnd})$.

In contrast to increasing λ, increasing Δ monotonically turns the vector field of auxiliary system (14) counterclockwise since for system A^+ (A^-) with $y > 0$ ($y < 0$) $\partial(A^+/y)/\partial\Delta = 1/y < 0$ ($\partial(A^-/y)/\partial\Delta = -1/y > 0$). Therefore, for a fixed $\lambda^* \in [\lambda_{Hsd}, \lambda_{Hnd})$ it makes limit cycle L_{osc} monotonically grow in the size. Formally introducing some function $f(\lambda, \Delta)$ that captures the monotonic decrease and increase of $d_G(\lambda, \Delta)$ in λ and Δ, respectively, we arrive at the statement of Claim B. □

Remark 1. While Proposition 2 provides a qualitative description of the dependence of d_G on λ and Δ, an analytical derivation of the exact form of function $f(\lambda, \Delta)$ and the explicit value of λ_{Hnd} is out of reach for the non-integrable auxiliary system (14). However, analytical lower and upper bounds on λ_{Hnd} can be given (see Proposition 3). Central to our study of partial ε-synchronization, the existence of function $f(\lambda, \Delta)$ with the properties detailed in Proposition 2 demonstrates the existence of a threshold value of $\lambda = \lambda_{Hnd}$ and, therefore, of inertia β beyond which increased inertia starts affecting the size of trapping region G_{trap}.

Proposition 3 (quantitative bounds). *Bifurcation value λ_{Hnd} used in Proposition 2 can be bounded as follows:*

$$\lambda_{dn} < \lambda_{Hnd} < \lambda_{up}, \quad \textit{where} \tag{23}$$

$$\lambda_{dn} = 2(a^2 - \Delta^2)^{1/4} \textit{ and } \lambda_{up} = 2\sqrt{(\Delta + 1)/\arcsin\frac{\Delta}{a}}.$$

Proof. The lower bound λ_{dn} corresponds to a critical value of λ at which fixed point e_1, being a stable node of system A^+, becomes a degenerate node, prior to turning into a stable focus. The type and stability of fixed point e_1 of A^+ can be evaluated through the equation $\ddot{\theta} + \lambda\theta + a\sin\theta = \Delta$ that yields the characteristic equation $\kappa^2 + \lambda\kappa + \sqrt{a^2 - \Delta^2} = 0$, evaluated at $\theta_{e_1} = \arcsin\frac{\Delta}{a}$ and obtained by applying a trivial algebraic expression. The roots of the characteristic equation are

$$\kappa^{\pm} = -\lambda/2 \pm \sqrt{\lambda^2/4 - \sqrt{a^2 - \Delta^2}}, \tag{24}$$

therefore, fixed point e_1 of system A^+ becomes a stable degenerate node with repeated eigenvalue $\kappa^{\pm} = -\lambda/2$ at $\lambda = \lambda_{dn} = 2(a^2 - \Delta^2)^{1/4}$. Equation (24) also indicates that the transition from a stable node fixed point of A^+, corresponding to λ_{Hnd} to the degenerate node and further to a stable focus is induced by decreasing λ, thereby demonstrating that $\lambda_{dn} < \lambda_{Hnd}$.

The upper bound λ_{up}, at which the trajectory T_{e_2} emanating from point e_2 at $y > 0$ is guaranteed to approach fixed point e_1 and, therefore, to form the upper part of heteroclinic contour L^{∞}_{nd} (see the proof of Proposition 1 for the details), can be derived via a directing Lyapunov function. Let $V(\theta, y) = 0$ represent the line l : $y = -\frac{\lambda}{2}(\theta - \theta_{e_1})$ which passes through fixed point e_1. Its negative slope $-\lambda/2$ was chosen to place the line between two eigenvectors $\boldsymbol{E}_l = \kappa^+(\theta - \theta_{e_1})$ and $\boldsymbol{E}_n = \kappa^-(\theta - \theta_{e_1})$ of stable node e_1, where eigenvector $\boldsymbol{E}_n$ with a steeper negative slope represents the stronger (non-leading) direction and is tangent to the non-leading stable manifold W_n [see the inset of Fig. 2(f)]. In this way, line l is designed to play the role of W_n in directing the trajectory T_{e_2} to fixed point e_2. Toward this goal, we shall show that the vector field of system A^+ transversely intersects line l in the downward direction so that the trajectory T_{e_2} is confined to reach fixed point e_2. To do so, we calculate the derivative of function $V = y + \frac{\lambda}{2}(\theta - \theta_{e_1})$ along trajectories of system A^+ (15) such that $\dot{V}|_{V=0} = \dot{y} + \frac{\lambda}{2}\dot{\theta}|_{V=0}$, which yields

$$\dot{V}|_{V=0} = \begin{cases} \Delta - \lambda y - \sin\theta + \lambda y/2 & \text{for } \theta \in (-\theta_{e_1}, 0], \\ \Delta - \lambda y - a\sin\theta + \lambda y/2 & \text{for } \theta \in [0, \theta_{e_1}), \end{cases} \tag{25}$$

where y is to be replaced with $y = -\lambda(\theta - \theta_{e_1})/2$. To prove that line l : $V(\theta, y) = 0$ is a directing Lyapunov function for trajectory T_{e_2}, we need to find the conditions under which $\dot{V} < 0$. Thus, transforming (25), we set

$$\begin{aligned} &\lambda^2(\theta_{e_1} - \theta)/4 > \Delta - \sin\theta \text{ for } \theta \in [-\theta_{e_1}, 0], \\ &\lambda^2(\theta_{e_1} - \theta)/4 > \Delta - a\sin\theta \text{ for } \theta \in [0, \theta_{e_1}]. \end{aligned} \tag{26}$$

Without attempting to solve this set of transcendental inequalities, we derive an upper bound on λ that guarantees that inequalities (26) are satisfied. To do so, we require the left-hand side (LHS) of (26), $\lambda^2\theta_{e_1}/4$, evaluated at $\theta = 0$ to be larger than the worst case scenario maximum of the right-hand sides (RHS), $\Delta + 1$, achieved at $\theta = -\pi$. In graphical terms, this sufficient condition implies that the line represented by the LHS with a θ-intercept at $\theta = \theta_{e_1}$ crosses the y-coordinate axis at a point that is higher than the maximum $\Delta + 1$ of graph $\Delta - \sin\theta$ and, therefore, the line is located above the graphs of the RHS function for any $\theta \in (-\theta_{e_1}, \theta_{e_1})$. This condition yields $\lambda^2 > 4(\Delta + 1)/\theta_{e1}$. Thus, replacing $\theta_{e1} = \arcsin\frac{\Delta}{a}$, we conclude that for $\lambda > \lambda_{up} = 2\sqrt{(\Delta + 1)/\arcsin\frac{\Delta}{a}}$, the vector field of auxiliary system (14) crosses line l transversely in the downward direction, thereby guaranteeing the presence of heteroclinic contour L^{∞}_{nd}. □

Remark 2. To explicitly express the conditions of Proposition 2 in terms of the auxiliary system's parameters, λ_{Hnd} in Claim A (Claim B) should be replaced with the upper (lower) bound λ_{up} (λ_{dn}) from (23).

Having characterized the properties of trapping region G_{trap} of auxiliary system (14), we shall now connect the conditions on its size to ε-synchronization within coherent cluster C_{osc} of system (1).

IV. PARTIAL SYNCHRONIZATION: THE MAIN RESULT

Recall that the existence of trapping region G_{trap} of auxiliary system (14) implies that the trajectories of each system $(\dot{\theta}_{ij}, \dot{y}_{ij})$ from (7) with $i, j = 1, \ldots, N_{osc}$ and initial conditions $\dot{\theta}_{ij}(0) = \theta_0$, $\dot{y}_{ij}(0) = y_0$, where $(\theta_0, y_0) \in G_{trap}$ are trapped inside G_{trap} for any t. While the dynamics of auxiliary system (14) inside trapping region G_{trap} are proved to be periodic, the behavior of each system $(\dot{\theta}_{ij}, \dot{y}_{ij})$ (7) inside G_{trap} may be richer and may be chaotic. What matters in this context is that the size of trapping domain G_{trap}, d_G, determined by (21) and (22), bounds the maximum phase difference between oscillators i and j from coherent cluster C_{osc}, so that $\dot{\theta}_{ij}(t) < d_G$, i, $j = 1, \ldots, N_{osc}$ for any t. Therefore, ε-synchronization within cluster C_{osc} is guaranteed to be stable when $d_G \leq \varepsilon$. Applying this argument to Propositions 2 and 3, we arrive at the main statement of this paper.

Proposition 4 (sufficient conditions for partial synchronization). *Partial ε-synchronization in the second-order Kuramoto system (1) is stable if the minimum normalized natural frequency mismatch between clusters C_{osc} and C_{rot}, $\delta > 1$, where δ is defined in (17) and* *(a) for* $\lambda > \lambda_{up} = 2\sqrt{(\Delta+1)/\arcsin\frac{\Delta}{a}}$, *where* $\lambda = 1/\sqrt{\beta K}$ *and a is defined in (11), the maximum normalized frequency mismatch within cluster* C_{osc}

$$\Delta < \Delta_{cr} = \left(\frac{N_{osc}}{N}\cos\varepsilon - \frac{N_{rot}}{N}\right)\sin\frac{\varepsilon}{2}, \tag{27}$$

where Δ *is defined in (16).*

(b) For

$$\lambda < \lambda_{dn} = 2(a^2 - \Delta^2)^{1/4} \tag{28}$$

the maximum normalized frequency mismatch $\Delta < g(\lambda)$, *where* $g(\lambda)$ *is a monotonically increasing function over* $\lambda \in (0, \lambda_{dn})$ *with* $g(0) = 0$.

Proof. In accordance with Definition 1, to prove the stability of partial ε-synchronization, we need to show that the phase differences between oscillators from coherent cluster C_{osc} remain bounded by ε, whereas the phase difference between any oscillator from C_{osc} and any oscillator from incoherent cluster C_{rot} whirls from $[-\pi, \pi]$. Demonstrating the later property for $\delta > 1$ is straightforward [see the paragraph after (17)]. The proof of the former property under conditions of Claim A and B directly follows from Propositions 2 and 3 and Remark 2. Condition (27) for Δ_{cr} follows from (21) solved for Δ for $d_G = \varepsilon$ and a from (11). Function $\Delta = g(\lambda)$ with the monotonic dependence on λ in Claim B is a level of function (22) with $d_G = \varepsilon$. □

Remark 3. As $\Delta > 0$ and $\varepsilon \in [0, \pi)$, sufficient condition (27) is only valid for $\varepsilon < \frac{1}{2}\arccos\frac{N_{rot}}{N_{osc}}$, and, therefore Proposition 4 is only applicable to $N_{osc} > N_{rot}$.

Remark 4. Proposition 4 is applicable to time-varying natural frequencies $\omega_i(t)$, provided that inequalities (27) and (28) are satisfied for each frequency distribution $\omega_i(t)$, $i = 1, \ldots, N$ with a given $\Delta(t)$ at any time t.

Remark 5. Bound (28) suggests the existence of a threshold value of λ and, therefore of inertia β beyond which increased inertia starts playing a desynchronizing role and reduces the maximum allowed frequency mismatch Δ for a fixed synchronization precision parameter ε (the blue solid line in Fig. 1). Remarkably, the actual, numerically validated dependence of Δ on λ (the blue dashed line in Fig. 1) also indicates critical values of λ close to λ_{dn} below which decreased λ effectively decreases Δ, although this dependence is not as sharp as the one guaranteed by sufficient condition (28).

While Proposition 4 guarantees that oscillators from cluster C_{rot} have whirling phases with respect to those from oscillatory cluster C_{osc}, it does not guarantee that the oscillators within C_{rot} remain incoherent. However, in all of our extensive simulations reported in Figs. 3 and 4, the rotatory phases of oscillators from C_{rot} always remained desynchronized. Figure 3 indicates this common case of incoherent whirling oscillators from C_{rot} and ε-synchronized oscillators within oscillatory cluster C_{osc}. The parameter values used in the simulations of Fig. 3 satisfy the conditions of Proposition 4 (Claim A) with $\varepsilon = \pi/4$ chosen to maximize the allowed frequency mismatch Δ at 18% for a given λ. Note that the actual trapping region for the trajectories from coherent cluster C_{osc} has the shape that closely resembles the shape of the corresponding heteroclinic contour L^{∞}_{nd} in auxiliary system (14).

Finally, Fig. 4 gives broader, numerical validation of our analytical results and shows how the required precision of ε-synchronization within C_{osc} and inertia (via $\lambda = 1/\sqrt{\beta K}$) control the maximum allowed natural frequency mismatch. In particular, Fig. 4 provides quantitative support for the bounds of Proposition 4 and demonstrates that the auxilary system captures the dynamics of system (1) quite well. The discrepancy between the analytical bound for stable partial synchronization depicted by curve H_{sd} and

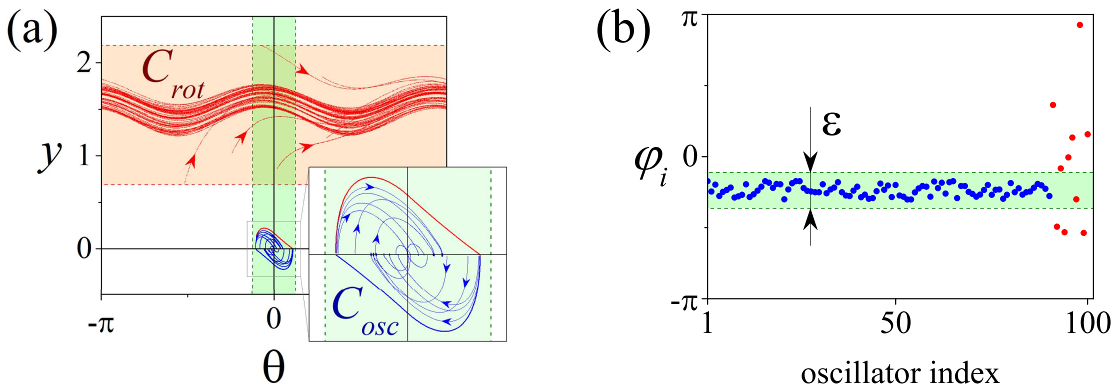

FIG. 3. Stable partial synchronization in network (1) of 100 oscillators with $N_{osc} = 90$ and $N_{rot} = 10$. (a). Representative trajectories of oscillators from coherent cluster C_{osc} (blue) and from incoherent cluster C_{rot} (red). The green strip displays the maximum phase difference ε between oscillators from cluster C_{osc}. The light red strip indicates the established range of phase velocities within incoherent cluster C_{rot}. The inset details the shape of the trapping region, determined by heteroclinic contour L^{∞}_{nd} of auxiliary system (14) for chosen $\lambda = 1.6 > \lambda_{Hnd}$ and $\Delta = 0.18$. (b) Snapshot of the corresponding spatiotemporal pattern at time $t = 100$ (10^5 iterations with step $h = 0.001$). The blue and red dots indicate the instantaneous phases of oscillators within clusters C_{osc} and C_{rot}, respectively. The green strip corresponds to that in (a). Natural frequencies ω_i, $i = 1, .., N_{osc}$ and ω_k, $k = 1, .., N_{rot}$ are randomly chosen from $[10 - \Delta, 10 + \Delta]$ and $[14.2 + \Delta, 15 + \Delta]$, respectively. Initial phases φ_i, $i = 1, .., N_{osc}$ are equally distributed within $[-\pi, \pi]$. Initial phases φ_k, $k = 1, .., N_{rot}$ are chosen randomly within $[-\pi, \pi]$. Initial velocities within coherent cluster C_{osc} are set to 0.1, and within incoherent cluster C_{rot} are chosen randomly from $[-1, 1]$.

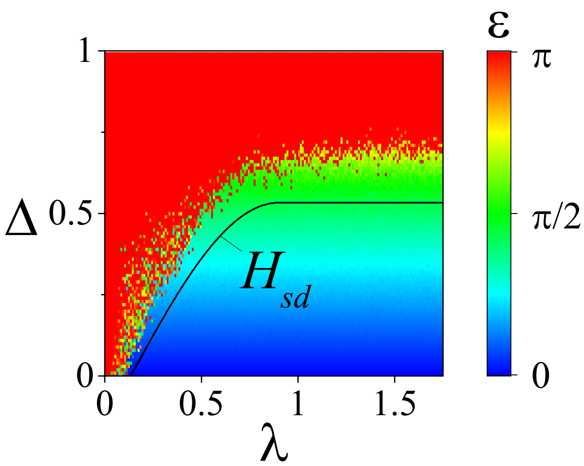

FIG. 4. Stability diagram for ε-synchronization within cluster C_{osc} as a function of maximum normalized frequency mismatch Δ and damping $\lambda = 1/\sqrt{\beta K}$. The color bar depicts the maximum phase difference ε of the established oscillations. The red region represents unstable synchronization corresponding to whirling phase differences within C_{osc}. Synchronization within incoherent cluster C_{rot} is always unstable for any pairs (λ, Δ) from the given range and distribution of natural frequencies and initial conditions and, therefore, its corresponding (λ, Δ) diagram would be all red and is not shown. Note a threshold-like dependence of Δ on λ such that increasing λ beyond $\lambda \approx 0.75$ does not effectively influence the stability of ε-synchronization within C_{osc}. Black curve H_{sd} corresponds to the emergence of trapping region G_{trap} in auxiliary system (14) and predicts the threshold-like effect remarkably well. Network size is $N = 100$ with $N_{osc} = 90$ and $N_{rot} = 10$. Natural frequencies ω_i, $i = 1, .., N_{osc}$ and ω_k, $k = 1, .., N_{rot}$ are randomly chosen from $[10 - \Delta, 10 + \Delta]$ and $[12.01, 14.01]$, respectively. All initial phases are chosen randomly from $[-\pi, \pi]$. Initial velocities are chosen as in Fig. 3.

the actual stability boundary originates from the construction of the auxiliary system that required the replacement of the coupling terms in system (1) with their upper bounds. As a result, partial synchronization in system (1) becomes stable prior to the formation of the trapping region in the auxiliary system (curve H_{sd}). Figure 4 also confirms that our analytical prediction that decreasing inertia β (via increasing λ) has a saturating effect on the maximum frequency mismatch that still supports synchronization within coherent cluster C_{osc}. The corresponding effective threshold on λ essentially indicates when partial synchronization in second-order Kuramoto model (1) becomes insensitive to decreased inertia and its stability conditions are the same as in the classical, first-order Kuramoto model. Somewhat surprising, this threshold-like transition takes place around the value of $\lambda = 0.7$, which is much lower than large values of λ (small values of inertia) at which a perturbation theory argument could suggest that stability conditions for partial synchronization in the first-order and second-order Kuramoto models become nearly identical.

V. CONCLUSIONS

Partial synchronization in the first and second-order Kuramoto models of heterogeneous oscillators is often viewed as a proxy for understanding the emergence of chimera states in networks of identical oscillators. In this paper, we have contributed to an improved analytical understanding of the conditions under which partial synchronization in the second-order finite-dimensional Kuramoto model emerges as a function of intrinsic oscillator frequency mismatches, inertia, and the relative size of coherent and incoherent clusters. To this end, we have developed the auxiliary system method, which transforms the multi-dimensional Kuramoto model to a set of coupled pendulum-type equations and then replaces their coupling terms with a bound that decouples the equations. This procedure yields a piecewise-smooth auxiliary system whose trajectories govern oscillating dynamics of the phase differences within the coherent cluster and rotating dynamics of the phase differences between oscillators from the coherent cluster and oscillators from the incoherent state. Of particular importance for the auxiliary system is the existence of a trapping region, which is formed by either a limit cycle or heteroclinic contours. The size of the trapping domain controls the maximum phase difference ε between coherent oscillators and yields explicit bounds that relate the maximum allowed natural frequency mismatch and phase differences with inertia and the size of the coherent cluster. Remarkably, these bounds have predicted threshold-like stability loss of partial synchronization with increasing inertia. A similar saturating effect of moderate inertia on the minimum critical coupling required for the formation of the coherent cluster has been previously studied numerically.[66] Our results provide analytical support to this numerical study and articulate the threshold-like role of inertia on the maximum allowed frequency mismatch via explicit analytical bounds.

Our sufficient conditions do not describe the dynamics of the phase differences between the oscillators from the "incoherent" cluster whose phases may become synchronized while rotating with respect to the phases of the coherent cluster. We have not observed any phase-locking within the incoherent clusters for the bimodal frequency distribution used in our numerical stimulation. However, choosing close natural frequencies within the incoherent cluster may induce this intra-cluster phase-locking between the rotating phase differences. The related limiting case of identical natural frequencies within the incoherent state can be well captured by a partial synchronization pattern with the incoherent cluster composed of only one oscillator. This pattern represents a solitary state[68,69] with one oscillator's phase rotating with respect to the rest of the network. The bounds of Proposition 4 guarantee the stability of this solitary state with $N_{rot} = 1$.

Similarly, by setting $N_{rot} = 0$, we obtain bounds for complete ε-synchronization in the second-order Kuramoto model. In contrast to partial synchronization in finite-size networks, analytical conditions for the stability of complete synchronization in the finite-dimensional heterogeneous Kuramoto model with inertia have been previously derived.[35,79] A comparative analysis of these conditions and our bounds applicable to complete synchronization when $N_{rot} = 0$ is beyond the scope of this paper.

Our auxiliary system method can be applied to analytically characterize (i) the formation of finer cluster partitions within the coherent cluster in the presence of an incoherent state and (ii) cluster synchronization with multiple coherent clusters with distinct inter- and intra-cluster oscillatory phase dynamics. Going beyond the all-to-all coupling studied in this paper, it can be potentially extended to handle more complex network topologies much in the vein of the analysis of frequency synchronization in the second-order Kuramoto model on a star graph.[73] These problems are a subject of future study.

ACKNOWLEDGMENTS

We dedicate this paper to the memory of Vadim S. Anishchenko, an outstanding scientist and an amazing friend. This work was supported by the Ministry of Science and Higher Education of the Russian Federation under Grant No. 0729-2020-0036, by the Russian Science Foundation under Grant No. 19-12-00367 (numerics; to N.V.B., V.N.B., and G.V.O.) and by the National Science Foundation (USA) under Grant Nos. DMS-1909924 and CMMI-2009329 (to I.V.B.).

AUTHOR DECLARATIONS

Conflict of Interest

The authors have no conflicts to disclose.

DATA AVAILABILITY

The data that support the findings of this study are available from the corresponding author upon reasonable request.

REFERENCES

[1] S. H. Strogatz, Nature **410**, 268 (2001).
[2] A. Pikovsky, M. Rosenblum, and J. Kurths, *Synchronization: A Universal Concept in Nonlinear Sciences* (Cambridge University Press, 2003), Vol. 12.
[3] S. Camazine, J.-L. Deneubourg, N. R. Franks, J. Sneyd, E. Bonabeau, and G. Theraulaz, *Self-Organization in Biological Systems* (Princeton University Press, 2003), Vol. 7.
[4] S. Boccaletti, V. Latora, Y. Moreno, M. Chavez, and D.-U. Hwang, Phys. Rep. **424**, 175 (2006).
[5] K. Schindler, C. E. Elger, and K. Lehnertz, Clin. Neurophysiol. **118**, 1955 (2007).
[6] C. Hammond, H. Bergman, and P. Brown, Trends Neurosci. **30**, 357 (2007).
[7] R. Roy and K. S. Thornburg, Jr., Phys. Rev. Lett. **72**, 2009 (1994).
[8] A. E. Motter, S. A. Myers, M. Anghel, and T. Nishikawa, Nat. Phys. **9**, 191 (2013).
[9] L. M. Pecora and T. L. Carroll, Phys. Rev. Lett. **80**, 2109 (1998).
[10] S. Boccaletti, J. Kurths, G. Osipov, D. Valladares, and C. Zhou, Phys. Rep. **366**, 1 (2002).
[11] V. N. Belykh, I. V. Belykh, and M. Hasler, Physica D **195**, 159 (2004).
[12] I. Belykh, E. de Lange, and M. Hasler, Phys. Rev. Lett. **94**, 188101 (2005).
[13] T. Nishikawa and A. E. Motter, Proc. Natl. Acad. Sci. USA **107**, 10342 (2010).
[14] V. N. Belykh, I. V. Belykh, and M. Hasler, Phys. Rev. E **62**, 6332 (2000).
[15] V. N. Belykh, I. V. Belykh, and E. Mosekilde, Phys. Rev. E **63**, 036216 (2001).
[16] A. Pogromsky and H. Nijmeijer, IEEE Trans. Circuits Syst. I: Fundam. Theory Appl. **48**, 152 (2001).
[17] A. Pogromsky, G. Santoboni, and H. Nijmeijer, Physica D **172**, 65 (2002).
[18] I. Belykh, V. Belykh, K. Nevidin, and M. Hasler, Chaos **13**, 165 (2003).
[19] M. Golubitsky and I. Stewart, Bull. Am. Math. Soc. **43**, 305 (2006).
[20] Y. Wang and M. Golubitsky, Nonlinearity **18**, 631 (2004).
[21] L. M. Pecora, F. Sorrentino, A. M. Hagerstrom, T. E. Murphy, and R. Roy, Nat. Commun. **5**, 4079 (2014).
[22] I. Belykh and M. Hasler, Chaos **21**, 016106 (2011).
[23] H. Kamei and P. J. Cock, SIAM J. Appl. Dyn. Syst. **12**, 352 (2013).
[24] F. Sorrentino, L. M. Pecora, A. M. Hagerstrom, T. E. Murphy, and R. Roy, Sci. Adv. **2**, e1501737 (2016).
[25] M. Golubitsky, I. Stewart, and A. Török, SIAM J. Appl. Dyn. Syst. **4**, 78 (2005).
[26] Y. Kuramoto, in *International Symposium on Mathematical Problems in Theoretical Physics* (Springer, 1975), pp. 420–422.
[27] S. H. Strogatz, Physica D **143**, 1 (2000).
[28] J. A. Acebrón, L. L. Bonilla, C. J. P. Vicente, F. Ritort, and R. Spigler, Rev. Mod. Phys. **77**, 137 (2005).
[29] E. Barreto, B. Hunt, E. Ott, and P. So, Phys. Rev. E **77**, 036107 (2008).
[30] E. Ott and T. M. Antonsen, Chaos **18**, 037113 (2008).
[31] H. Hong, H. Chaté, H. Park, and L.-H. Tang, Phys. Rev. Lett. **99**, 184101 (2007).
[32] A. Pikovsky and M. Rosenblum, Phys. Rev. Lett. **101**, 264103 (2008).
[33] Y. Maistrenko, O. Popovych, O. Burylko, and P. Tass, Phys. Rev. Lett. **93**, 084102 (2004).
[34] O. V. Popovych, Y. L. Maistrenko, and P. A. Tass, Phys. Rev. E **71**, 065201 (2005).
[35] F. Dörfler and F. Bullo, SIAM J. Appl. Dyn. Syst. **10**, 1070 (2011).
[36] E. A. Martens, E. Barreto, S. Strogatz, E. Ott, P. So, and T. Antonsen, Phys. Rev. E **79**, 026204 (2009).
[37] C. R. Laing, Physica D **238**, 1569 (2009).
[38] Y. Kuramoto and D. Battogtokh, Nonlinear Phenom. Complex Syst. **5**, 380 (2002).
[39] D. M. Abrams and S. H. Strogatz, Phys. Rev. Lett. **93**, 174102 (2004).
[40] D. M. Abrams, R. Mirollo, S. H. Strogatz, and D. A. Wiley, Phys. Rev. Lett. **101**, 084103 (2008).
[41] M. J. Panaggio and D. M. Abrams, Nonlinearity **28**, R67 (2015).
[42] L. Larger, B. Penkovsky, and Y. Maistrenko, Phys. Rev. Lett. **111**, 054103 (2013).
[43] N. Semenova, A. Zakharova, V. Anishchenko, and E. Schöll, Phys. Rev. Lett. **117**, 014102 (2016).
[44] N. Semenova, G. Strelkova, V. Anishchenko, and A. Zakharova, Chaos **27**, 061102 (2017).
[45] M. Bolotov, G. Osipov, and A. Pikovsky, Phys. Rev. E **93**, 032202 (2016).
[46] M. Bolotov, L. Smirnov, G. Osipov, and A. Pikovsky, Chaos **28**, 045101 (2018).
[47] E. A. Martens, S. Thutupalli, A. Fourrière, and O. Hallatschek, Proc. Natl. Acad. Sci. U.S.A. **110**, 10563 (2013).
[48] T. Kapitaniak, P. Kuzma, J. Wojewoda, K. Czolczynski, and Y. Maistrenko, Sci. Rep. **4**, 6379 (2014).
[49] I. Belykh, R. Jeter, and V. Belykh, Sci. Adv. **3**, e1701512 (2017).
[50] A. M. Hagerstrom, T. E. Murphy, R. Roy, P. Hövel, I. Omelchenko, and E. Schöll, Nat. Phys. **8**, 658 (2012).
[51] M. R. Tinsley, S. Nkomo, and K. Showalter, Nat. Phys. **8**, 662 (2012).
[52] Z. G. Nicolaou, H. Riecke, and A. E. Motter, Phys. Rev. Lett. **119**, 244101 (2017).
[53] O. E. Omelchenko, Nonlinearity **26**, 2469 (2013).
[54] M. Wolfrum, O. E. Omelchenko, S. Yanchuk, and Y. L. Maistrenko, Chaos **21**, 013112 (2011).
[55] C. R. Laing, Phys. Rev. E **100**, 042211 (2019).
[56] P. Ashwin and O. Burylko, Chaos **25**, 013106 (2015).
[57] M. J. Panaggio, D. M. Abrams, P. Ashwin, and C. R. Laing, Phys. Rev. E **93**, 012218 (2016).
[58] B. Ermentrout, J. Math. Biol. **29**, 571 (1991).
[59] L. Tumash, S. Olmi, and E. Schöll, Chaos **29**, 123105 (2019).
[60] H.-A. Tanaka, A. J. Lichtenberg, and S. Oishi, Phys. Rev. Lett. **78**, 2104 (1997).
[61] H.-A. Tanaka, A. J. Lichtenberg, and S. Oishi, Physica D **100**, 279 (1997).
[62] P. Ji, T. K. Peron, F. A. Rodrigues, and J. Kurths, Sci. Rep. **4**, 4783 (2014).
[63] V. Munyaev, L. Smirnov, V. Kostin, G. Osipov, and A. Pikovsky, New J. Phys. **22**, 023036 (2020).
[64] M. Komarov, S. Gupta, and A. Pikovsky, Europhys. Lett. **106**, 40003 (2014).
[65] S. Olmi, Chaos **25**, 123125 (2015).
[66] S. Olmi, A. Navas, S. Boccaletti, and A. Torcini, Phys. Rev. E **90**, 042905 (2014).
[67] I. V. Belykh, B. N. Brister, and V. N. Belykh, Chaos **26**, 094822 (2016).
[68] P. Jaros, S. Brezetsky, R. Levchenko, D. Dudkowski, T. Kapitaniak, and Y. Maistrenko, Chaos **28**, 011103 (2018).
[69] Y. Maistrenko, S. Brezetsky, P. Jaros, R. Levchenko, and T. Kapitaniak, Phys. Rev. E **95**, 010203 (2017).
[70] B. N. Brister, V. N. Belykh, and I. V. Belykh, Phys. Rev. E **101**, 062206 (2020).

[71] G. S. Medvedev and M. S. Mizuhara, J. Stat. Phys. **182**, 1 (2021).
[72] C. R. Laing, Chaos **19**, 013113 (2009).
[73] V. N. Belykh, M. I. Bolotov, and G. V. Osipov, Model. Anal. Inf. Syst. **22**, 595 (2015).
[74] A. A. Andronov, A. A. Vitt, and S. E. Khaikin, *Theory of Oscillators: Adiwes International Series in Physics* (Elsevier, 2013), Vol. 4.
[75] M. di Bernardo, C. Budd, A. Champneys, and P. Kowalczyk, *Piecewise-Smooth Dynamical Systems: Theory and Applications* (Springer, 2007).
[76] V. N. Belykh, N. V. Barabash, and I. V. Belykh, Chaos **29**, 103108 (2019).
[77] V. N. Belykh, N. V. Barabash, and I. V. Belykh, Chaos **31**, 043117 (2021).
[78] L. N. Belyustina and V. N. Belykh, Differ. Equ. **9**, 403 (1973).
[79] Y.-P. Choi, S.-Y. Ha, and S.-B. Yun, Physica D **240**, 32 (2011).